Smart Mater. Struct. **21** (2012) 065013 (8pp) doi:10.1088/0964-1726/21/6/065013

A bidirectional shape memory alloy folding actuator

Jamie K Paik[1] **and Robert J Wood**[2]

[1] School of Engineering, Ecole Polytechnique Federale de Lausanne, Switzerland
[2] School of Engineering and Applied Sciences, Harvard University, USA

E-mail: jamie.paik@epfl.ch

Received 1 November 2011, in final form 19 March 2012
Published 22 May 2012
Online at stacks.iop.org/SMS/21/065013

Abstract
This paper presents a low-profile bidirectional folding actuator based on annealed shape memory alloy sheets applicable for meso- and microscale systems. Despite the advantages of shape memory alloys—high strain, silent operation, and mechanical simplicity—their application is often limited to unidirectional operation. We present a bidirectional folding actuator that produces two opposing 180° motions. A laser-patterned nickel alloy (Inconel 600) heater localizes actuation to the folding sections. The actuator has a thin (<1 mm) profile, making it appropriate for use in robotic origami. Various design parameters and fabrication variants are described and experimentally explored in the actuator prototype.

(Some figures may appear in colour only in the online journal)

1. Introduction

Shape memory alloys (SMAs) are attractive engineering materials due to their ability to memorize shapes through a thermally induced solid state phase transition [1, 2]. The material composition (e.g. Cu–Zn, Cu–Zn–Al, Cu–Al–Ni, Ni–Ti, Ni–Ti–Fe, Fe–Pt) largely determines the mechanical properties including ductility, corrosion, and 'memory' properties of the alloy. There are three categories of SMA shape changing effects that are derived from crystal reorientation during a reversible high-temperature austenite and low-temperature martensite phase change: the pseudoelastic effect, the one-way effect, and the two-way effect [3, 2]. The pseudoelastic effect exhibits no visible plastic deformation by temperature or through loading. The one-way effect is characterized by shape change upon loading, but no reorientation upon cooling. Once deformed, the 'memorized' shape is recovered when heated above the transition temperature. The two-way effect refers to shape change upon cooling and heating without external loading.

The one-way effect is the basis of most SMA actuators and often requires antagonistic springs or actuators to induce loading. The addition of antagonistic actuators is not an attractive solution for producing repeated motions because of added complexity. When applying a 'reverse' load, a preloaded spring or superelastic-NiTi element are popular methods to de-twin SMA actuators [4, 5]. However, to the authors' knowledge there is no example of a one-way SMA actuator that produces two motions in a single device. The two-way effect is desirable as an actuator property because it allows repeated shape changes with temperature control without an antagonist. However, upon variable loading, the two-way effect is minimized, and its strain is not as pronounced as in the one-way effect.

Therefore, for the application of robotic origami [1, 6] that requires multiple sequential foldings of tiled sheets, we seek low-profile actuators which use a single actuator in recovering the original shape.

In this paper, we present the design and fabrication of a compact SMA bidirectional actuator that produces two opposing rotational motions with a high torque density and a low profile. The actuator's two rotational axes are nearly co-linear and each capable of up to 180° of rotation. The SMA bidirectional actuator is activated by a thin external heater that allows focused heating designed specifically for this application.

2. Related work

The choice of actuator for modular robots in general, and robotic origami in particular, is a critical aspect of design. For robotic origami [1, 6], the actuator must

conform to submillimeter geometry of a tiled sheet while producing enough torque to create a sequence of foldings. SMA actuators are common in applications that have strict geometric restrictions. Son introduced a linearity enhanced SMA wire actuator with reverse hysteresis control to minimize the shape variation [7]. Similarly, Constanza's nitinol one-way shape memory springs are controlled using a detailed thermomechanical characterization and actuator design [8]. A previously reported low-profile torsional actuator produces a high torque but only in a single direction [1]. In another example, a wearable supportive device enhances facial expressiveness with an SMA wire actuator [9]. Some millimeter-scale linear micro-actuators use bent ribbons of thin SMA and produce 420–570 μm deflection depending on the antagonistic spring design [10]. While this deflection is impressive considering the scale, there are challenges with scaling up as it will be difficult to use without the silicon wafer backing. These examples of SMA actuators are suitable for their specific millimeter-scale tasks but not applicable for robotic origami without significantly altering the current tiled sheet design.

In order to produce multiple shapes from the same origami, the sheet must be flat before being activated into a new shape. This requires each folding edge to fold in two directions (in and out). We can consider embedding two single direction actuators at a cost of additional mechanisms and weight. Some SMA actuators can produce two shapes by using mechanical compliance to move between minimum energy shapes upon activation. Kohl presented a millimeter-scale gas microvalve made with a sputter-coated SMA thin film. Its photo-etched shape and different composition allows an increased transition temperature [11]. However, the thin film application of SMA is yet to be applicable for deflections larger than 1 mm. Tung's laser-machined design of SMA tubing makes a catheter structure compliant in desired directions (with a high deflection) with sensors made of superelastic SMA [12]. However, it only produces motion in one direction. Actuators that use the two-way effect typically have bistable shapes and often require no antagonistic structure. Mineta designed a 8 μm two-way actuator by sputter coating TiNiCu and flat annealing the structure [13]. Their actuator is made of SMA thin film that is appropriate for nanoscale gripping. This design is difficult to scale up since the strain increases proportionally to the size and the thickness of the structure. Kim *et al* presented a two-way shape memory effect in their millimeter-scale SMA that is usually unstable under loading. They showed that by inducing compressive loading cycles, it is possible to create more robust two phase shapes by 'training' the material [14]. This process may be applicable for thicker and larger scale actuators but for low-profile actuators, the effect of the cyclic loading process is uncertain and requires extensive material treatment. For thinner materials this could cause additional fatigue and even early stress fractures.

An actuator with a high torque density and a low profile is more achievable in using thin films, springs, and ribbons of SMAs. However, it is extremely rare to find a structure or actuator that enables robust, active bidirectional actuation without having antagonistic structure or manual loading. Ancillary loading mechanisms often add to the overall volume of the actuation system and net power consumption as the active actuator must overcome the 'reverse' loaded system to produce desired work. Our design maintains a low profile and enables bidirectional motions in a single 500 μm thick actuator.

3. Bidirectional actuator design and fabrication

The complexity in designing a multi-directional SMA actuator is in creating distinct motions using a single material. The most versatile actuator would produce multi-directional actuation along collinear axes, or axes which intersect at a single point, a trait which is especially valuable for small-scale applications. The presented bidirectional actuator design minimizes the separation of two actuating axes without interfering with the resulting torque and range of motion. The engineering challenge lies in creating distinct activation areas which can be annealed, fabricated, and actuated.

3.1. Design choices

The majority of SMA actuators use Joule heating to excite the phase transition. This is a common method to actuate SMA actuators because of its design and control simplicity. However, due to the inherently low resistivity of metal-based SMA materials, substantial current is typically required. This high current can cause problems for associated electrical traces due to I^2R losses. Previously, the authors proposed an alternative heating method for SMA actuators that uses an external heater made of coiled Ni–Cr to generate heat [1]. This method showed superior power efficiency and response times compared to Joule heating due to its ability to focus the heating area while requiring significantly lower currents. Pertaining to the actuator performance, the heating method is irrelevant provided that sufficient heating is supplied. However, a localized activation method is required for a bidirectional actuator or any thermally activated multi-directional SMA actuator because they require concentrated heating in selected regions of movement. With conventional Joule heating, producing selective heating is difficult as discrete current paths are difficult to achieve.

Our designs for low-profile actuators rely on thin NiTi sheets and an annealing process as described below. The SMA material thickness is directly proportional to the torque output (i.e. the folded and annealed cross-sectional area is proportional to the produced torque). Although high torque-to-volume is almost always desirable in rotary actuators, the thickness of the SMA sheet material is limited by the maximum strain of the material. Figure 1 shows the 2D outline of the actuator and its dimensions along with the heater. We use 0.1 mm thick sheets which are compatible with our machining and annealing techniques. This thickness is also appropriate for conductive heating from the external heater that can initiate the thermally activated actuator within seconds.

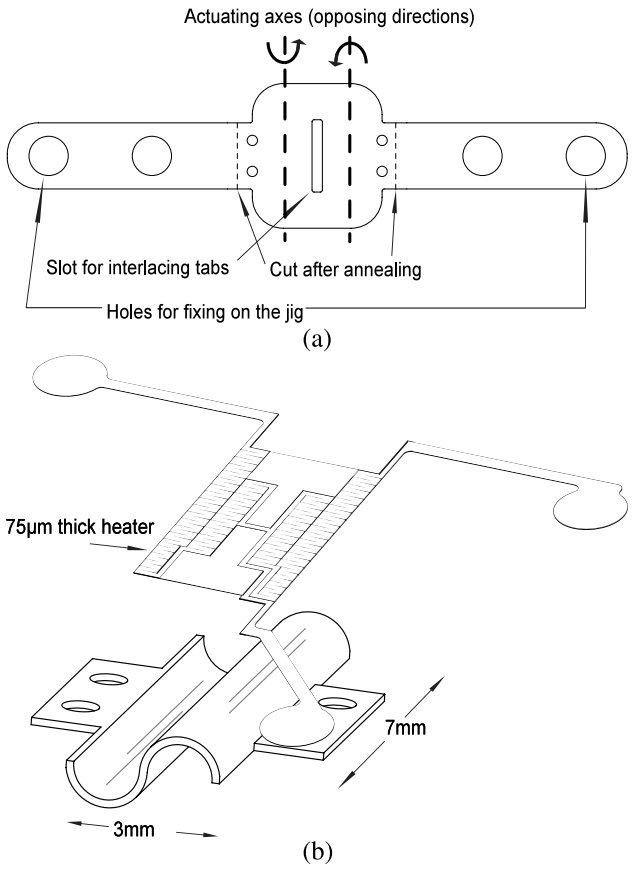

Figure 1. Schematics of the bidirectional SMA actuator. Laser-machined outline of the actuator (a), heater and actuator dimensions (b).

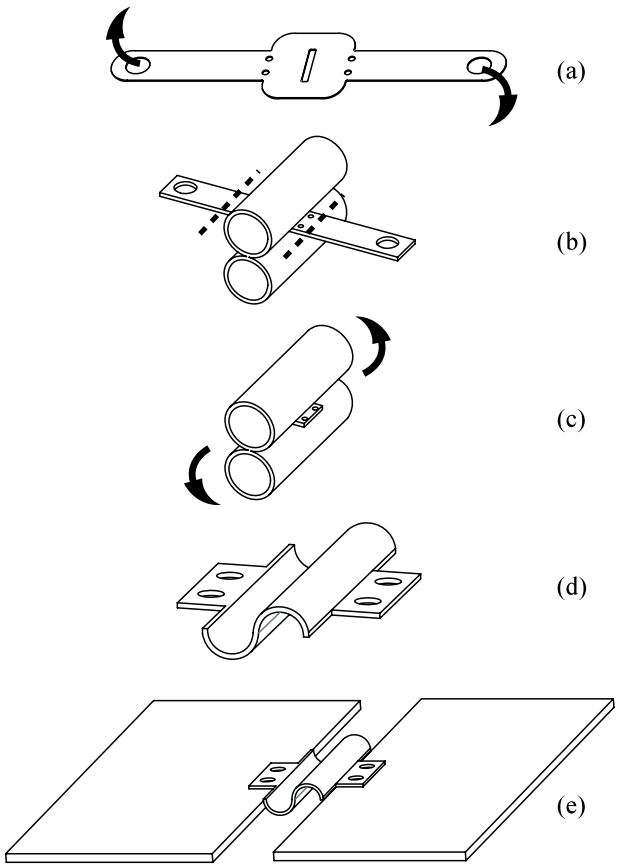

Figure 2. Schematics of the bidirectional SMA actuator fabrication. Laser-machined actuator outline from SMA sheet (a), opposingly interlaced tabs for creating uniform curvature for bidirectional actuating regions: here the tabs are used to anchor the shape (b), once removed from the jig the tabs are trimmed (c), each actuating region is unfolded (d), and the actuator is mounted along the folding axis between tiles of a robotic origami structure (e).

3.2. Fabrication process

The actuator is composed of an SMA folding substrate and a heating element. The SMA sheet is laser machined while flat, then folded and annealed to create new memorized shapes in different regions. As a result of the combination of 2D machining and folding, the designer can create a large range of motions as reported in [1]. We also propose unique solutions to thermal activation with a heating element and attachment to the NiTi SMA, which is notorious for its poor solderability.

3.2.1. Actuator. Our design focuses on creating two opposing torques in a single actuator while keeping the axes of rotation close so that two torques would be nearly collinear. We used NiTi sheets with a transition temperature of 65 °C (0.1 mm M alloy from Memry-Metale GmbH (www.memry.com)). To . form a desired 3D shape, we followed the annealing process established in [1]. In the case of a single actuator producing a 180° folding motion, dowel pins prescribed the radius of curvature. However, for the bidirectional actuator, we incorporated features into the design to produce a consistent radius of curvature without tooling by introducing sacrificial tabs and slots. Figure 1 illustrates a laser-machined SMA sheet with two actuating regions and their rotation of axes. The radius of curvature was governed by the length of the material between the slot and the tab. We chose this to be 3 mm making the radius of curvature to be less than a quarter of a millimeter. This relationship is characterized by the length of the active region which forms a circle made when rolled up. Therefore, having the slot in the center allowed two ends of the tab to interlace to form a tight and consistent curvature during and after annealing (figure 2). We used a jig to anchor the two ends and maintain the shape. The jig was designed with a socket-head cap screw spaced by spherical washers on each end that controls a lever arm with multiple sets of pegs (figure 3). We applied constant pressure on the actuator by adjusting the force of the lever arm. The entire jig is placed in a furnace preheated to 400 °C for 30 min and then removed and quenched to room temperature in running tap water. Once removed from the jig, the tabs were removed from the slot by unfolding the actuating axes. The long tabs were trimmed off close to the bolt holes.

3.2.2. Flex-heater. Having a heating element that concentrates heating at a specific area is critical for the bidirectional SMA actuator. We have experimented with two ways of fabricating the heater. One was by directly attaching or 'printing' the heater on the actuator body

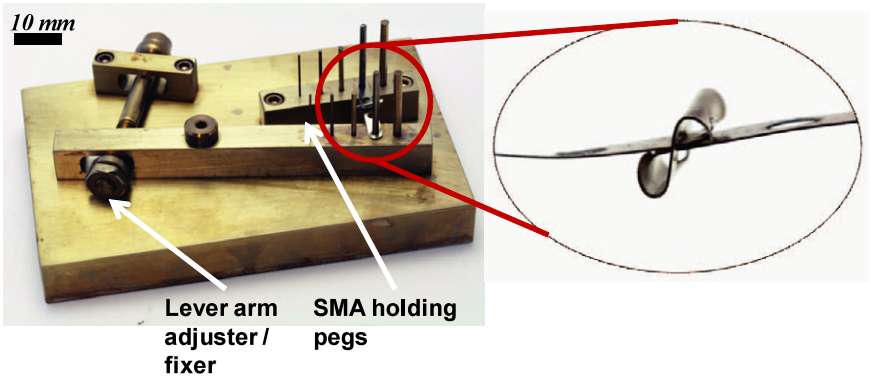

Figure 3. Annealing jig for maintaining shape during annealing. The inset shows the actuator when the tabs are interlaced and placed on the jig.

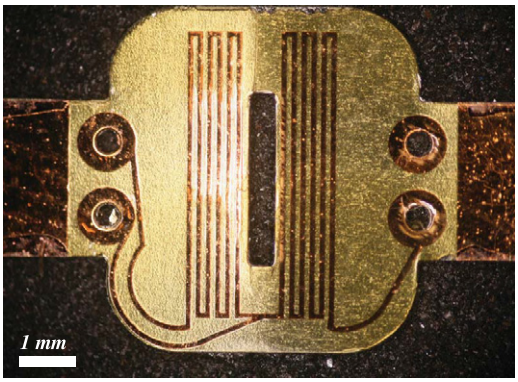

Figure 4. 'Printed-on' heater on the surface of the SMA actuator.

in the pre-annealed state and another was by attaching a heater after fabrication. For the 'printed-on' heater, we sandwiched the heating path between layers of insulators. We spin-coated (Specialty Coating Systems, Spincoat G3P-8) the laser-machined SMA with an adhesion promoter (T9039 HD MicroSystems). Once vapor-cured under nitrogen gas (Rapid Thermal Processor, RTP-600xp), it was again spin-coated with polyimide precursor HD 4110 which has a maximum operating strain of 40%. Polyimide precursors are spin-coatable and can achieve a uniform thickness (about 2–3 μm) on the substrate surface. The insulated SMA was then oxygen plasma treated before being placed in a vacuum chamber for sputter coating. We sputter-coated Cr and Cu (0.01 and 0.1 μm respectively) and dry-etched the heater patterns using a DPSS laser. A second polyimide layer was used for insulation (figure 4).

However, this 'printed-on' heater delaminated when under high strains associated with the current annealing method (approximately 10% strain, limited by the fracture strain of the NiTi sheet). This solution was applicable for lower strain cases when using thinner substrates or a larger radius of curvature. For the given dimensions of the current bidirectional actuator (that produces approximately 20% strain), we designed an external heater made of polyimide-Inconel 600 (72% Ni, 14–17% Cr, and 6–10% Fe). With a polyimide layer as a backing (35 μm polyimide and 40 μm Inconel 600), we followed a similar process to flex-circuit fabrication to make a flexible heating layer. We first coated the Inconel 600 sheet in photoresist (Shipley 24D positive photoresist). The negative heater path design was directly exposed to a DPSS UV laser and etched with $FeCl_3$. The heater outline was then cut out from the sheet using the same laser. The heater has two separate resistive paths for two activation regions of the bidirectional actuator (each had a resistance 33 Ω and consumed 0.07 W to reach 75 °C within 2 s). We designed each heater to share the ground

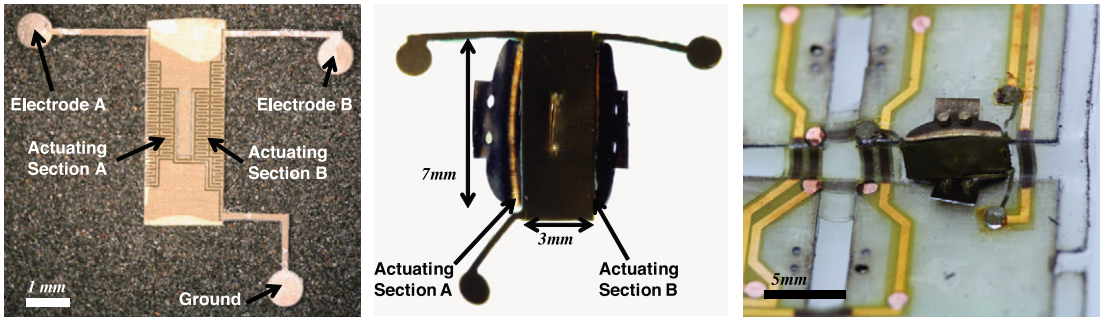

(a) (b) (c)

Figure 5. Inconel heater with an SMA actuator. Patterned Inconel heater with three electrodes, before (a) and after (b) mounting to an actuator. The bidirectional SMA actuator module on a robotic origami prototype (c).

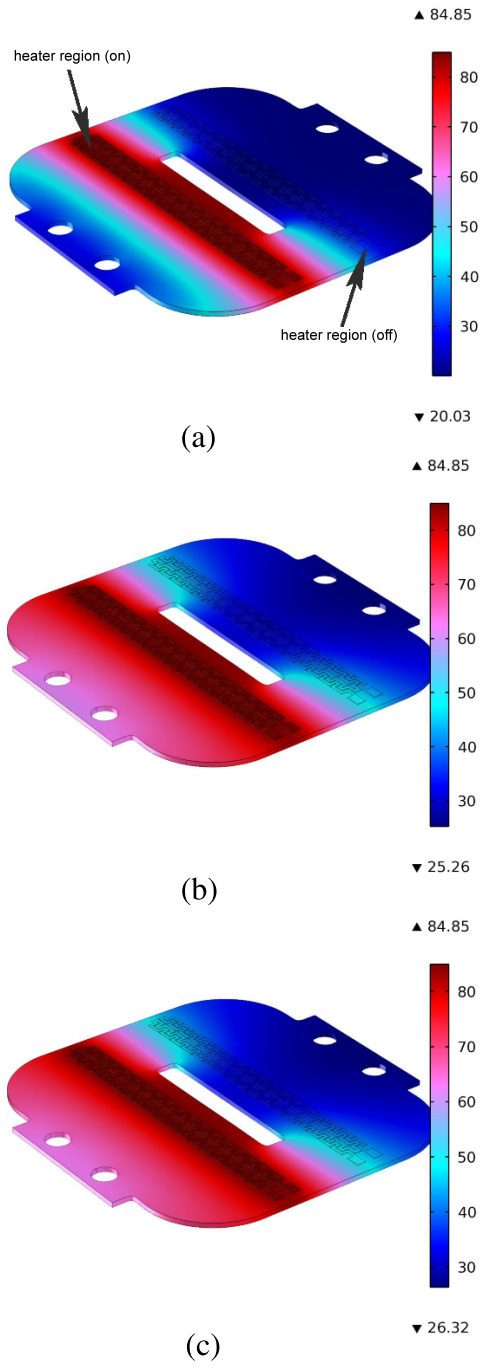

Figure 6. COMSOL simulation of (a) the heater model, 0.1 s heater activation, (b) the epoxy bonded heater model (epoxy thickness 0.08 mm), and (c) the epoxy bonded heater model (epoxy thickness 0.12 mm).

line to minimize solder connections (see figure 5(a)). The electrode ends were 1 mm circles that were soldered onto flex circuits mounted to the origami platform (figure 5(b)). This heater was mounted face down on the actuator's folding sides (see figure 5(c)). The heater path design, and wire and electrode positions were customized for power consumption and to match the geometry of the actuator substrate.

Bonding the flex-heaters to the SMA substrate was a challenge as NiTi is notorious for its poor solderability. Due to the thin geometry and high strains, most pliable epoxies or pressure sensitive adhesives failed after a single use. We observed improved bonding of the heaters using a microlaser welder (Laser Star's Nd:YAG laser welder with a minimum spot size 200 μm). To compliment the welds, we used a two-part epoxy that was thermally conductive and electrically insulating (Cast-Coat Inc.'s CC3-300 with 40% maximum elongation). For the prototypes, we used a thin layer of epoxy to place the flex-heater first and welded the perimeter to the NiTi substrate.

4. Actuator modeling

We predict the behavior of the presented SMA actuator by (a) heat flow modeling to explore the effect of one heater on the adjacent section and (b) thermomechanical modeling of the response of the actuator to temperature changes. As we discussed in section 3, we used a combination of laser-welding and adhesive to bond the heater to the actuator body and compared the heating speed for different adhesive thicknesses. For the bidirectional SMA actuator, isolated heating regions are critical for producing independent motions. This is a challenge that is exacerbated by the requirement that the rotational axes be in close proximity to mimic collinear rotations. We created COMSOL models with two sections of actuation which were actuated by two Inconel circuits. We ran the model with three different adhesive thicknesses all operating at the same power input 0.075 W at 0.22 A (0, 0.08, and 0.12 mm). We also observed the change of the heater temperature with time.

Figure 6(a) shows the temperature distribution at 0.1 s when the left heater was turned on. The activation region was above the alloy's transition temperature, 65 °C. We observed minimal effect of the adhesive thickness variation on the temperature distribution (see figures 6(b) and (c)). These temperature distribution graphs are the simulations after 20 s of heating. The effect of epoxy thickness was only equivalent to 5% variation of the nominal power. We observed that the temperature in the unheated region stayed below the transition temperature (even after 20 s) while the active regions required less than 2 s to activate. The middle slot in the actuator served as a mechanically critical feature during annealing and provided thermal isolation of the two actuating regions. In COMSOL, we observed that above 100 °C the heater temperature started to affect the opposite region.

In order to model the thermomechanical effect of the SMA actuator, we assume that the strain is isolated along the axes of rotation and assume that the shape memory effect of each axis is independent of the other. Our analysis splits the SMA into thin layers and integrates the contribution of each layer to estimate the phase transition induced strain. Following the stress–strain and phase transformation model of Leclercq *et al* [15], the strained area was assumed to be passive and experiencing the thermomechanical coupling effect through heat input q in (1) where q, C_v, λ, ΔT, Δu are the applied thermal power, specific heat capacity, thermal conductivity coefficient, Laplacian temperature, and phase

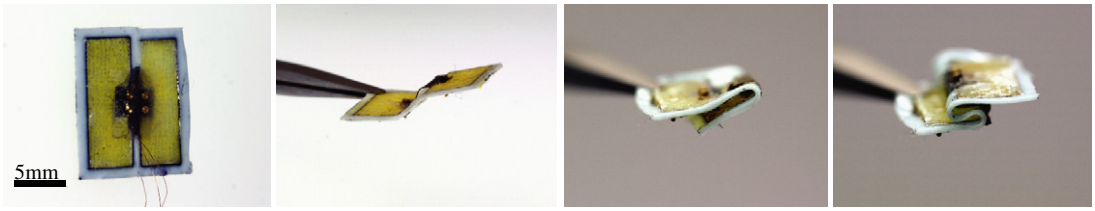

Figure 7. Bidirectional actuator modes: before activation (a) and (b), single axis activated (c) and both axes activated (d).

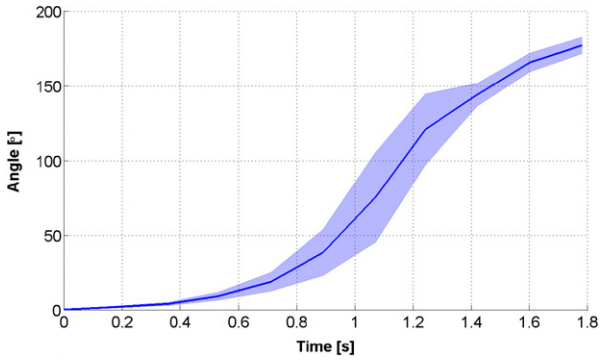

Figure 8. Angle response of four samples to a step input current; the shaded area indicates one standard deviation.

transformation latent heat respectively.

$$\rho(C_v\dot{T} - \Delta u\dot{z}) = q + \lambda\Delta T. \tag{1}$$

In this energy balance equation [16], the thermal power input from the heater dictates the rate of change of the volume fraction of martensite phase, z, and the temperature change, and the last term of the equation depends on the external temperature.

Each layer of the actuator that is a distance y from the neutral axis has a strain as shown in (2), (3), where θ is the bending angle of the actuator, l is the length of the actuating section, and R is the radius of curvature where R_0 is the radius of curvature at the neutral axis

$$R_0 = \frac{l}{\pi} \qquad \text{and} \qquad R = \frac{l}{\pi + \theta} \tag{2}$$

$$\varepsilon_x(y) = \left(\frac{y}{R} - \frac{y}{R_0}\right) = \frac{y\theta}{l}. \tag{3}$$

The stress generated in each layer due to bending is given as (4) where E is the average Young's modulus of all the phases and A is the cross-sectional area of the hinge that was assumed to be constant during the transformation

$$\sigma_x(y) = E(\varepsilon_x(y) - \gamma z_\sigma(y)). \tag{4}$$

The changes of z_σ (volume fraction of deformed martensite) and z_T (twinned martensite) are approximated functions of the cosine of temperature change [17, 18]. Here, γ is the pseudo-plastic deformation coefficient and z is the volume fraction of martensite. The torque generated (5) by the actuator is equivalent to the total moment generated by integrating the contribution of each infinitesimal layer

$$M = A\int_0^t \sigma_x y \, \mathrm{d}y. \tag{5}$$

5. Actuator experimental evaluation

The mechanical design and annealing process dictates the performance of the SMA actuators. The bidirectional SMA actuator inherits most of the properties from a previously demonstrated single-axis torsional actuator [1], but with the additional challenge of multiple thermal activation regions in a single actuator. Therefore, it is critical to have both regions thermally isolated from each other. The COMSOL modeling described in section 4 predicts that the bidirectional actuator should produce independent actuation at 65 °C (at 0.06 W per region). However, even at 85 °C, we found that the actuator produced a faster response without interfering with its bidirectional functionality. Figure 7 displays two modes of the bidirectional actuator where selective heating enables the user to actuate one or two opposing sides simultaneously.

In order to evaluate typical actuator metrics, we tested prototypes with the maximum heater temperature at 85 °C on one side of the actuator. On average, we found the full range of motion of 0°–180° was achieved within 2 s. Figure 8 displays the angular position of four prototypes under a step current input. Repeated testing on a single actuator showed little difference in the full actuation time. This number was a vast improvement from a NiCr coil heater prototype that took about twice the time to produce the same range of motion [1]: the thin and flat design of the Inconel heater produced concentrated heating to effectively thermally activate the actuator. Motion data were taken using a video and the deflection angle was collected using ProAnalyst motion analysis software.

Measuring the angular response to temperature change, we found the actuator displayed the shape memory effect even before it reached the phase transition temperature. However, the maximum angular deflection was observed at the transition temperature of 65 °C. Figure 9 shows the actuator behavior at power input of 0.09 W. At this input power, the actuator reaches the transition temperature within 1.8 s. When varying the power input, the transition trend was the same but the temperature ramp decreased or increased with the current supply.

However, the maximum angular deflection was observed at the transition temperature as shown in figure 9. When

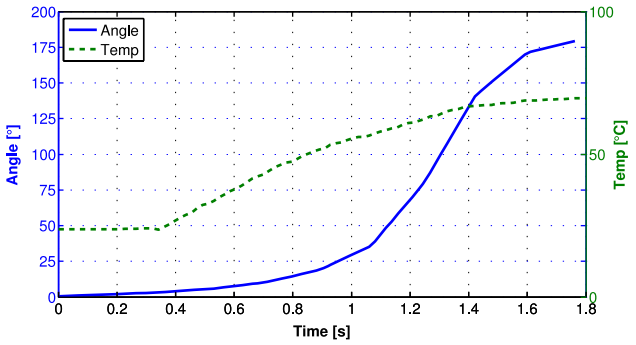

Figure 9. Temperature and angular displacement of the actuator.

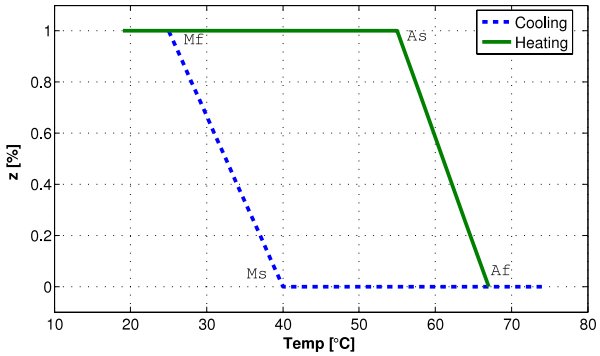

Figure 10. Martensite-phase start and finish temperatures and austenite-phase start and finish temperatures. Idealized curves extrapolated from experimental phase transition observations.

Table 1. NiTi material properties.

Property	Symbol	Value
Specific heat capacity	C_v	49 J kg^{-1}
Thermal conductivity	λ	10 W mK^{-1}
Young's modulus (average of all phases)	E	42 MPa
Pseudo-plastic deformation coefficient	γ	0.05
Mass density	ρ	6500 kg m^{-3}

varying the power input, the transition trend was the same but the temperature ramp was slower when less current was supplied or faster when increased.

The thermomechanical model of the prototype required material-specific phase transformation temperatures. We found these temperatures experimentally during heating and cooling post-annealed samples and observing their shape memory effect (figure 10).

We used the pseudo-plastic deformation coefficient given by the manufacturer (see table 1) . These values determined the rate of change from martensite to austenite. The video images produced the measured strain values by measuring curvature and using the relationship in (2) (figure 11). The maximum strain of 20% was achieved at 180° deflection. The calculated and measured curves had comparable slopes.

We measured the blocked torque of the actuator and compared it to the values found by (5). We used the experimental setup used in [1] where the distal portion of

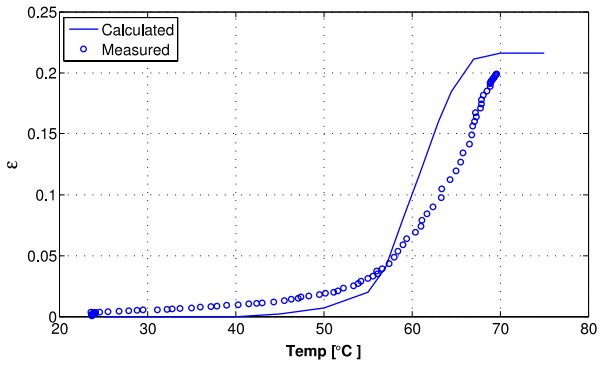

Figure 11. Measured and calculated strain values when supplied with 0.075 W at 0.22 A.

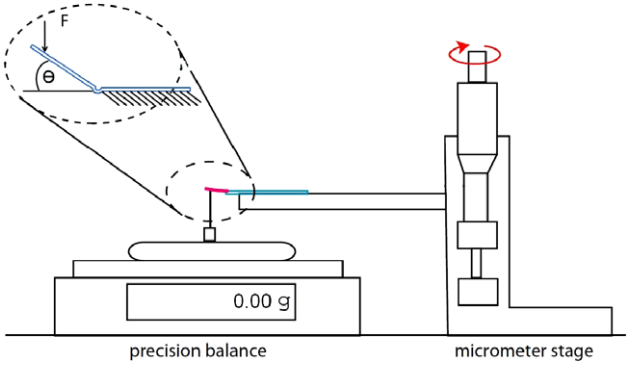

Figure 12. Experimental setup for measuring blocked torque. The exerted force on the balance is recorded for corresponding angular deflection [1].

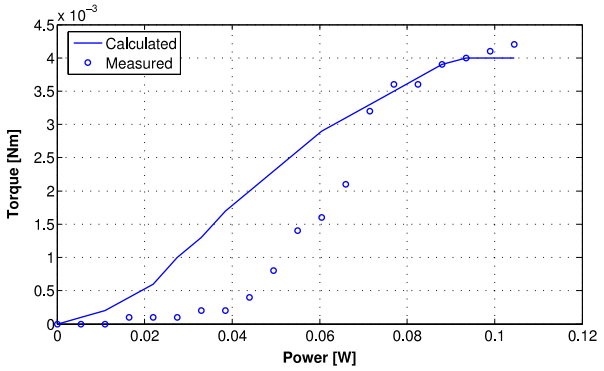

Figure 13. Measured and calculated torques.

the actuator exerts a force on a precision scale (figure 12). The maximum torque was found when the actuator was lying flat on the balance point where the reading was recorded for varying power input. Figure 13 displays the exerted torque as a function of power input. We observe that a higher power input showed a better match with the theoretical values. When the power is small, the effect of power loss is more apparent and is observed by a relatively large gap between the calculated and measured plot. Table 2 summarizes the actuator specifications.

Table 2. Actuator specifications.

Property	Value
Range of motion	0°–180°
Mass (with heater)	0.05 g
Actuation time constant	≈1 s
Power consumption (no load)	0.092 W

6. Conclusion

This paper presents design considerations, fabrication processes, and experimental results of a bidirectional SMA actuator. Having an external heater as a thermal activation method, the actuator showed superior response time and power efficiency than conventional Joule-heated SMA actuators—with relevance to small-scale robotics applications. The thin heaters created selective heating that allowed the actuator to produce two distinct torques within a single actuator. The design of the actuator allowed for a simpler annealing process (compared even to a single-axis actuator [1]) while providing thermal isolation in two actuating regions. The unique low profile of the prototype is compatible with integration in a thin robotic origami structure.

Acknowledgments

This work was supported by the Defense Advanced Research Projects Agency (DARPA) under grant W911Nf-08-1-0228 (Programmable Matter) and the Wyss Institute for Biologically Inspired Engineering.

References

[1] Paik J, Hawkes E and Wood R 2010 A novel low-profile shape memory alloy torsional actuator *Smart Mater. Struct.* **19** 125014

[2] Kohl M 2004 *Shape Memory Microactuators* (Berlin: Springer)

[3] Van Humbeeck J, Chandrasekaran M and Delaey L 1991 Shape memory alloys: materials in action *Endeavour* **15** 148–54

[4] Koh J and Cho K 2010 Omegabot: biomimetic inchworm robot using SMA coil actuator and smart composite microstructures (SCM) *2009 IEEE Int. Conf. on Robotics and Biomimetics (ROBIO), IEEE* pp 1154–9

[5] Yang S and Seelecke S 2008 Modeling and analysis of SMA-based adaptive structures *Proc. COMSOL Conf., 2008 (Boston)*

[6] Hawkes E, An B, Benbernou N, Tanaka H, Kim S, Demaine E, Rus D and Wood R 2010 Programmable matter by folding *Proc. Natl Acad. Sci.* **107** 12441

[7] Son H, Tak C, Kang S, Kim J, Nam T and Lee Y 2010 Design and control of a linearity-enhanced SMA actuator *Phys. Scr.* **2010** 014059

[8] Costanza G, Tata M and Calisti C 2010 Nitinol one-way shape memory springs: thermomechanical characterization and actuator design *Sensors Actuators* A **157** 113–7

[9] Jayatilake D and Suzuki K 2010 A multiple SMA hybrid actuator to generate expressions on the face *2010 IEEE Int. Conf. on Robotics and Automation (ICRA), IEEE* pp 2203–8

[10] Kohl M and Skrobanek K 1998 Linear microactuators based on the shape memory effect *Sensors Actuators* A **70** 104–11

[11] Kohl M, Dittmann D, Quandt E and Winzek B 2000 Thin film shape memory microvalves with adjustable operation temperature *Sensors Actuators* A **83** 214–9

[12] Tung A, Park B, Liang D and Niemeyer G 2008 Laser-machined shape memory alloy sensors for position feedback in active catheters *Sensors Actuators* A **147** 83–92

[13] Mineta T, Kida N, Nomura S, Makino E, Sugawara T, Toh S and Shibata T 2008 Pulsation sensor integrated with microvascular holding actuator for thrombosis monitoring *Sensors Actuators* A **143** 14–9

[14] Kim H, Yoo Y and Lee J 2008 Development of a NiTi actuator using a two-way shape memory effect induced by compressive loading cycles *Sensors Actuators* A **148** 437–42

[15] Leclercq S and Lexcellent C 1996 A general macroscopic description of the thermomechanical behavior of shape memory alloys *J. Mech. Phys. Solids* **44** 953–7

[16] Abadie J, Chaillet N and Lexcellent C 2004 Bending model of an integrated SMA micro-actuator *J. Intell. Mater. Syst. Struct.* **15** 601

[17] Liang C and Rogers C 1997 Design of shape memory alloy actuators *J. Intell. Mater. Syst. Struct.* **8** 303–13

[18] Liang C and Rogers C A 1990 One-dimensional thermomechanical constitutive relations for shape memory materials *J. Intell. Mater. Syst. Struct.* **1** 207–34